Simulating the effect of Nature-based Solutions as a mitigation tool for Urban Heat Islands

Angelly de Jesus Pugliese Viloria[1], Maria Antonia Brovelli[1]

[1] Department of Civil and Environmental Engineering, Politecnico di Milano, Italy - angellyde.pugliese; maria.brovelli@polimi.it

Keywords: urban heat island, susceptibility mapping, machine learning, nature-based solutions

Abstract

The Urban Heat Island (UHI) effect is a phenomenon that typically occurs in areas with dense infrastructure and limited vegetation. Nature-based solutions (NbS) have been proposed to mitigate the effects of climate change and have been proved to reduce the frequency of its hazards. Therefore, this research examines how UHIs are influenced by the simulated implementation of NbS. The area of interest (AOI) of this study is the city of Milan in Northern Italy and the purpose of this research is two-fold. First, to train machine learning (ML) models to predict Surface UHI (SUHI) susceptibility and intensity, and their corresponding SUHI maps, based on land cover, Land Surface Temperature (LST), Normalised Difference Vegetation Index (NDVI), Normalised Difference Built-up Index (NDBI) and other ancillary data. Afterwards, the produced SUHI intensity ML model was re-evaluated to analyse the expected behaviour of simulated NbS, specifically for green roofs and parks. The NDVI, NDBI, and albedo of the simulated vegetation areas were changed to the average values of the urban vegetation in the City of Milan, 0.57, -0.17, and 0.15 respectively. The SUHI statistics of the specific areas of change were analysed pre and post simulation. The results showed that green roofs have the potential to lower SUHI intensity by 5 degrees Kelvin. The proposed methodology can be extended to simulate multiple scenarios based on specific needs.

1. Introduction

Cities concentrate the majority of the world’s population and due to the effects of climate change are facing rising temperatures, alteration in precipitation patterns, and extreme weather events (Lu et al., 2024). The ability of a city to withstand these challenges depends on the policies crafted by its leaders, which need to be based on reliable information. Hence, precise environmental assessments are essential to support resilience against climate-change related hazards.

Susceptibility quantifies the likelihood of hazardous events occurring at a particular location by evaluating its inherent physical and environmental characteristics (Bentivoglio et al., 2022). This analysis can be carried out using artificial intelligence methods, which treat the occurrences of hazards as the dependent variable and develop a model using independent conditioning factors, i.e., physical and environmental factors.

Urban areas have become ’islands’ of higher temperatures with respect to the rural outlying areas (Pugliese Viloria et al., 2024). This phenomenon is referred to as the Urban Heat Island (UHI) effect, which typically occurs in areas with dense infrastructure and limited vegetation. Specifically, UHIs are areas with greater temperature than the average temperature in rural areas. In this context, UHI susceptibility refers to the UHI likelihood in a specific location.

Nature-based solutions (NbS) have been proposed to mitigate the effects of climate change and have been proved to reduce the frequency and intensity of its derived hazards. The proposed NbS to alleviate Urban Heat Islands (UHIs) include enhancing urban greenery and albedo, such as implementing green roofs (He et al., 2021) and increasing urban vegetation (Calhoun et al., 2024). Therefore, the present research examines how UHIs are influenced by the simulated implementation of NbS. The simulated NbS, consisting of new urban vegetation areas, were introduced considering different patterns, in order to assess how different setups may influence UHI susceptibility.

The methodology section describes the case study area and the UHI modelling process which details the data analysis and preprocessing. Subsequently, the results section presents the UHI susceptibility model and map, the selection of the simulated vegetation areas, and the re-evaluation of the model considering the change.

2. Methodology

The area of interest (AOI) of this study, depicted in figure 1, is the city of Milan (in black) located in Northern Italy. It is surrounded by its metropolitan area (in red). The area of the city and the metropolitan area are 181 km^2 and 1575 km^2, respectively.

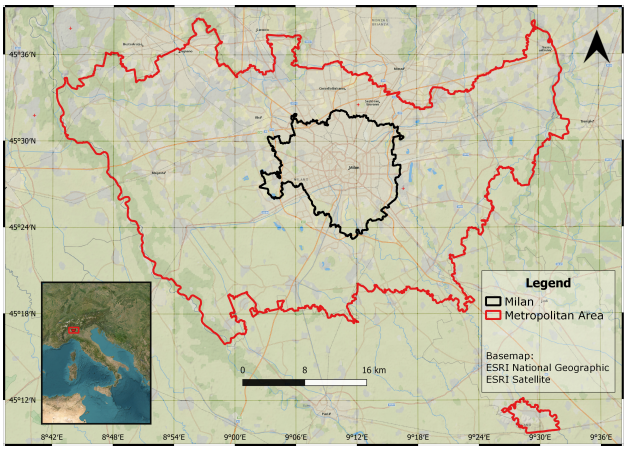

Figure 1. Area of interest

The purpose of this study is two-fold. First, Machine Learning (ML) models were trained to predict the Surface Urban Heat Island (SUHI) susceptibility and the SUHI intensity alongside their correspondent maps in the AOI. Second, Nature based Solutions (NbS), i.e., the introduction of vegetation areas, were simulated and the SUHI intensity was re-evaluated to measure the effect of the simulated changes.

The following four subsections detail the concept of SUHI modelling; the used data sources and preprocessing, i.e. Land Surface Temperature (LST) and Land Cover (LC); an analysis on the LST and LC dynamics; and a description on the NbS simulation and relevant concepts on the matter.

2.1 Surface Urban Heat Island susceptibility

Surface Urban Heat Island (SUHI) refers to the effect of urban islands of high surface temperature with respect to outlying rural and vegetation areas. In fact, the SUHI can be derived based on the Land Surface Temperature (LST) and the Land Cover (LC).

Considering the LST and the land cover class, the reference LST can be computed. The reference LST is the average LST in rural and vegetated areas. The SUHI can be computed using equation 1, where LST_p is the LST at each pixel and LST_r is the reference LST. The product of this computation is a binary SUHI map.

$$SUHI = \begin{cases} 1 & LST_p > LST_r \\ 0 & LST_p \leq LST_r \end{cases} \quad (1)$$

Moreover, the SUHI intensity is defined as the temperature difference between LST_p and LST_r, see equation.

$$SUHI_{intensity} = LST_r - LST_p \quad (2)$$

SUHI susceptibility was approached as a binary supervised classification based on SUHI maps derived from equation 1 to characterise the behaviour of the SUHI effect in the AOI. This classification is based on factors such as LST, LC, spectral indices and other ancillary data as independent variables; see 2.2 for further details. The workflow is detailed in figure 2.

Furthermore, the SUHI intensity was modelled to showcase the areas where the SUHI was more severe as a function of LC, spectral indices and ancillary data. The SUHI intensity model was used to evaluate the impact of NbS, independent from the LST. In fact, the model prescinds from the LST to prioritise the effect of vegetation if the SUHI intensity rather than the LST which has a high variability.

2.2 Data sources and preprocessing

The main data sources were Land Use Land Cover (LULC), Landsat-8 L2C2, and certain ancillary data which are described in detail in the following subsections. The spatial resolution of all the datasets was set to 5x5 m^2 to keep best spatial detail based on the available data.

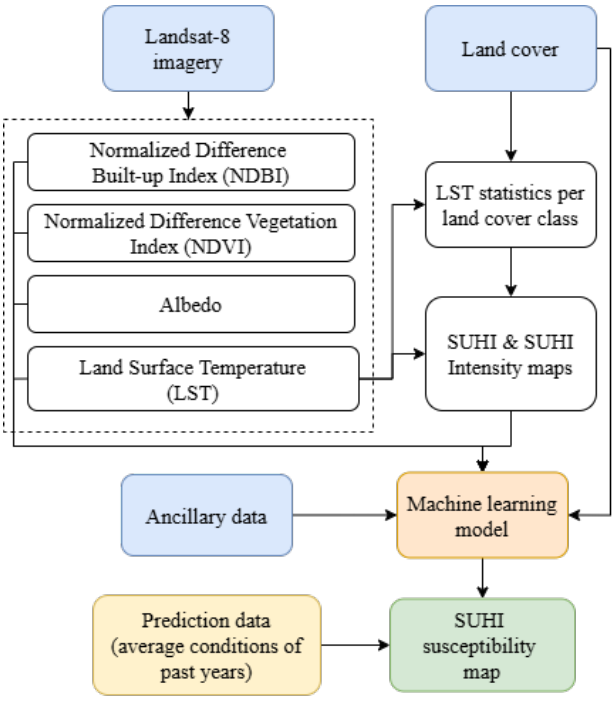

Figure 2. SUHI susceptibility modelling workflow.

2.2.1 Land Cover The Land Use/Land Cover (LULC) dataset is publicly provided by the Italian Lombardy Region agency and it is know as DUSAF, Agricultural and Forestry Land Use Destination for its initials in Italian. DUSAF LULC is derived from areal photographs and new versions of the DUSAF dataset have been released every three years since the year 2000. For the purpose of this study, the versions of the years 2015, 2018, and 2021 were used.

The DUSAF dataset is divided into five main classes which are eventually subdivided to provide more details on the land use. The main classes are man-made areas (1), agricultural areas (2), wooded areas and semi-natural environments (3), wetlands (4) and water bodies (5). However, an ad-hoc class set was used to better characterise the SUHI using a reduced number of classes. The ad-hoc class set definition can be found in the following list, and its representation on the city of Milan in figure 3.

1. Residential urban areas: continuous and discontinuous urban fabric
2. Industrial and abandoned urban areas: productive areas, large public establishments, private service facilities; quarrying areas, landfills, construction sites, sports and recreational areas, artificial and abandoned land.
3. Transportation infrastructure: Road and rail networks, ancillary spaces, ports, airports and heliports.
4. Urban green areas: parks, gardens, uncultivated green areas.
5. Agricultural areas: arable land, permanent crops, and permanent lawns.
6. Forest: forested areas including broad-leaved forest, coniferous forests, recent reforestations, and environments with evolving shrub and/or herbaceous vegetation.

7. Water bodies and wetlands: riverbeds, artificial watercourses, watersheds, and vegetation of inland wetlands and peat bogs.

8. Bare land: Dunes. Not present in the AOI.

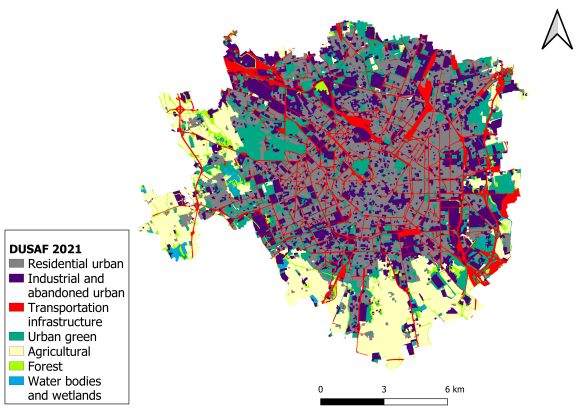

Figure 3. DUSAF Land Use Land Cover 2021 - reclassified

2.2.2 Landsat-8 L2C2 imagery The images were retrieved from 2015 - 2022 in the months of June, July, and August with a maximum 15% of cloud coverage and full coverage of the AOI. The total number of scenes is 17, with an average of two scenes per year (see the scene list in the Appendix). The year 2017 had imagery availability only in may, therefore, the scene was included as a reference but was not considered for furher computations. The Land Surface Temperature (LST), the Normalised Difference Vegetation Index (NDVI), the Normalised Difference Built-up Index (NDBI), the albedo, the SUHI and the SUHI Intensity were derived per each scene.

- The LST was extracted from Landsat-8 scenes using equation 3, where DN is the digital number of the thermal band (band 10).

$$LST(K) = 0.00341802 * DN + 149 \tag{3}$$

- The NDVI was computed using the red (R) and Near Infrared (NIR) bands, 4 and 5 respectively; see equation 4. The NDVI range is (-1:1) and indicates the vegetation greenness.

$$NDVI = \frac{NIR - R}{NIR + R} \tag{4}$$

- The NDBI was computed using the Near Infrared (NIR) and Shortwave Infrared SWIR 1 bands, 5 and 6 respectively; see equation 5. The NDBI range is (-1:1) and emphasises the built-up areas.

$$NDBI = \frac{SWIR_1 - NIR}{SWIR_1 + NIR} \tag{5}$$

- The albedo was computed using the blue (B), R, NIR, SWIR 1 and SWIR 2 bands; see equation 6. It provides an index on the capacity of a surface to reflect radiation.

$$albedo = 0,356 * B + 0,130 * R + 0,373 * NIR + 0.085 * SWIR_1 + 0.072 * SWIR_2 - 0.0018 \tag{6}$$

- The SUHI and SUHI intensity of each scene were computed using equations 1 and 2, where LST_p is the LST at each pixel and LST_r is the reference LST derived from the LST in the DUSAF LULC vegetation pixels, i.e., agricultural and and forested areas.

All these variables were averaged per year (mosaicked) to model the phenomenon. The Landsat-8 training set consisted of yearly summer scenes to avoid peak values due to either very extreme LST, and gap filling if few clouds and shadows were present.

2.2.3 Ancillary data Further data consists of building height, distance to main roads, distance to water bodies, and population density.

2.3 Land cover and land surface temperature dynamics

DUSAF LULC datasets were compared throughout the years 2015, 2018, and 2021. Figure 4 shows the areas per land cover class per year while figure 5 displays the class transition from 2015 to 2021, all in km^2. Slight changes can be observed in both graphs.

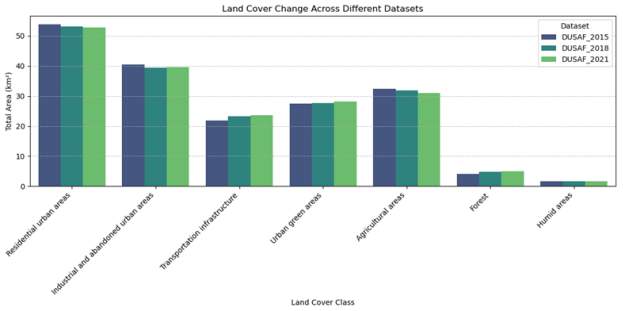

Figure 4. DUSAF land cover area per class

Residential urban areas have declined, primarily transforming into industrial zones, transportation infrastructure, and urban green areas. Similarly, industrial areas have shifted toward residential, transportation, and green spaces, reflecting broader urban development patterns. Transportation infrastructure has expanded, encroaching on agricultural land and forest, while urban green areas have grown at the cost of agricultural land. Agricultural areas have experienced significant reductions, with large portions being converted into forested land and urban green areas, suggesting a trend toward ecological restoration and reforestation. Forests and humid areas, although affected by other transitions, have seen modest increases, particularly as agricultural land is repurposed for environmental conservation. These changes highlight the ongoing interplay between urban expansion, environmental preservation, and land resource management.

Furthermore, figure 6 shows the LST per land cover class per each DUSAF LULC year, considering Landsat-8 scenes in the AOI. Specifically, for 2015: June 7th, July 22th, and August 7th; for 2018: July 30th and August 15th; for 2021: July 6th and July 22th. The plot shows a clear trend on LST with man-made areas

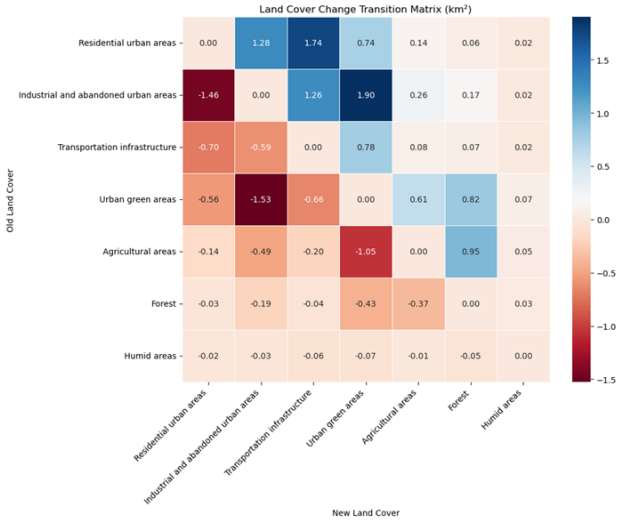

Figure 5. DUSAF land cover change matrix 2015-2021

(residential, industrial, and transportation infrastructure) reaching the highest values ranging from 315-320K, natural areas (agricultural, forest, water bodies) with the lowest values ranging from 309-315K, and urban green areas in the middle with a range of 314-318K.

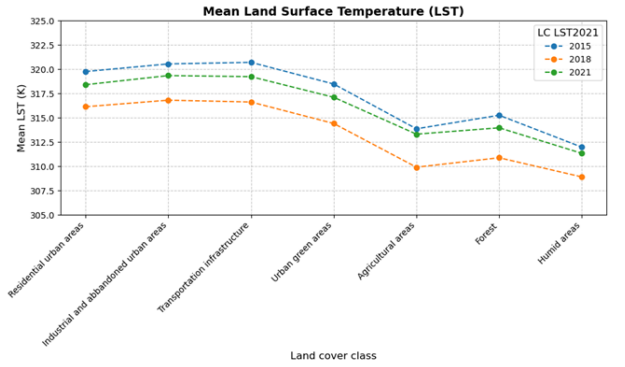

Figure 6. Average summer land surface temperature per land cover class [2015, 2018, 2021]

2.4 Nature-based Solutions Simulation

The simulation of Nature-based Solutions (NbS) consists of adding mocked vegetation areas to the LULC with the purpose of re-evaluating the SUHI intensity model to measure the variations. The scope of the NbS is limited to urban greenery, specifically parks and green roofs.

The new urban greenery can follow different patterns, i.e., following different traditional sampling techniques such as random, stratified, clustered, or systematic sampling. Nevertheless, in-depth vegetation pattern analyses such as Morphological Spatial Pattern Analysis (MSPA), can be used to understand their mitigation towards the UHI effect (Soille and Vogt, 2022).

2.4.1 Morphological Spatial Pattern Analysis The MSPA is a segmentation technique which provides a categorisation of the geometry and connectivity of a specific landscape. The result consists of 23 non-overlapping classes which can be simplified to Core, Islet, Perforation, Edge, Loop, Bridge, and Branch (Soille and Vogt, 2009).

The MSPA was used in the present research to interpret the current vegetation pattens. First, for each DUSAF LULC dataset (2015, 2018, and 2021) a binary vegetation/non-vegetation raster was created enclosing the urban green, agricultural and forest areas. Then, the GuidosToolbox (Vogt and Riitters, 2017) was used to compute the vegetation MSPA in each of the years, e.g., see the MSPA of 2021 in the AOI in figure 7.

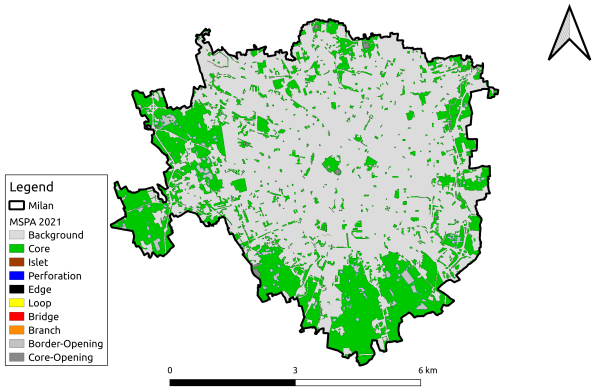

Figure 7. MSPA of vegetation in the city of Milan, 2021

The area change in the MSPA classes during 2015, 2018, and 2021 is reported in table 1. All the classes keep a stable area through the years. There is, however, a slight decrease in the background, i.e., non-vegetation decrease, and a slight increase on edges, core-openings, and border-openings.

MSPA class	2015	2018	2021
Background	114.92	114.13	114.35
Core	58.72	58.84	58.70
Islet	0.01	0.01	0.01
Perforation	0.49	0.50	0.49
Edge	4.50	4.73	4.80
Loop	0.01	0.01	0.01
Bridge	0.01	0.02	0.01
Branch	0.12	0.14	0.14
Core-opening	2.74	2.97	2.82
Border-opening	0.26	0.43	0.43

Table 1. MSPA of vegetation in the years 2015, 2018, and 2021 in km^2

The current MSPA vegetation patterns of 2021 were considered in the generation of the new vegetation areas.

3. Results

3.1 Surface Urban Heat Island modelling and mapping

The SUHI susceptibility was modelled using an artificial neural network (ANN) with the binary SUHI as target variable based on the LST, NDVI, LC, and ancillary data.

The sampling was carried out using the metropolitan area of Milan in order to provide more variability to the model. It consisted of randomly extracting 10.000 points per each yearly summer Landsat-8 mosaic resulting in approximately 70.000 points. The sampled points were constrained to be equally split into four classes: vegetated UHI, non-vegetated UHI, vegetated non-UHI, and non-vegetated non-UHI. The training/testing ratio was 80/20%.

The model produced an overall testing accuracy of 87%, precision 90%, recall 81%, and F1-score 86%. Furthermore, the Random Forest (RF) importances were computed with the previously described sampled data, see figure 8. The most important features, according to the RF model, were the LST with almost ∼70% of importance, followed, in a smaller proportion, by the NDVI and the population density. Furthermore, the land cover areas with the higher importance were the agricultural and urban green areas.

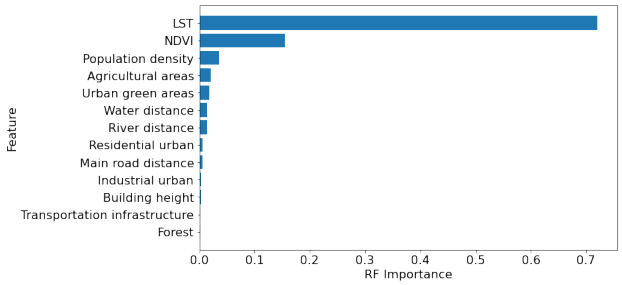

Figure 8. SUHI feature importance derived from Random Forest.

To predict the susceptibility, the inputs were the average LST and spectral indices from 2020 to 2022, with the purpose of showcasing the latest behaviour of the SUHI. The result of the model is the probability of SUHI, represented by class 1 in equation 1. See the SUHI susceptibility map in figure 9, the black outlined shape represents the city of Milan while the red outlined shape represents the metropolitan city of Milan with the purpose of showcasing areas with low SUHI susceptibility (in blue).

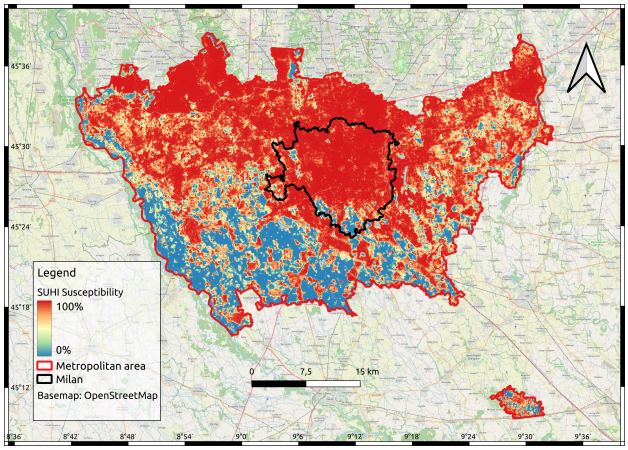

Figure 9. SUHI susceptibility in the Metropolitan City of Milan, Italy.

Furthermore, the SUHI intensity was modelled through an ANN regression. The training points and set up was the same as the previous model, excepting for the target change and the exclusion of LST. The model produced a mean absolute error of 2.65, a root mean squared error of 3.46, and a R^2 score of 0.5 in estimating the SUHI intensity in Kelvin. See the map in figure 10.

3.2 SUHI susceptibility vs. MSPA

The SUHI intensity (average conditions 2020-2022) and the vegetation MSPA of 2021 (figure 7) were used to extract the zonal statistics to understand the distribution of the UHI effect throughout the vegetation patterns. The results are presented in tables 2 and 3.

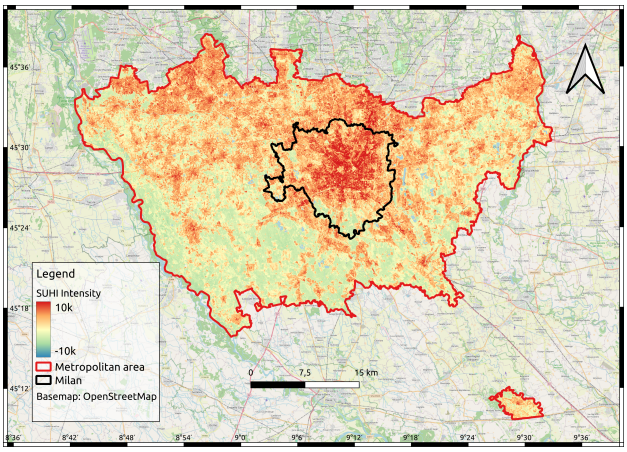

Figure 10. SUHI intensity in the Metropolitan City of Milan, Italy.

The results must be interpreted considering an AOI, corresponding to the city of Milan (181 km^2), and the area covered by each MSPA class (see table 1). Even if the Background and Core classes cover the 90% of the AOI, the zonal statistics were interpreted (tables 2 and 3). The role of core vegetation areas in reducing urban temperatures can be observed, having the lowest SUHI intensity (1.55 K). In contrast, fragmented and isolated vegetation patches, like Edges, exhibit higher SUHI intensity values, indicating reduced cooling efficiency. Vegetation corridors, such as bridges and branches, help mitigate SUHI by connecting green spaces and maintaining microclimate stability. The highest SUHI intensities were found in urbanized zones with sparse vegetation, emphasizing the need for expanding and connecting green infrastructure to enhance climate resilience.

Statistics	Backg.	Core	Islet	Perfor.	Edge
Mean	5.97	1.55	3.69	1.79	3.92
Std	2.93	3.01	2.43	2.43	2.42
Variance	8.59	9.06	5.89	5.91	5.84
Area (km²)	120.68	52.07	0.007	0.44	4.46
25^{th} Perc.	3.89	-1.00	1.82	0.02	2.43
50^{th} Perc.	6.11	1.90	4.03	1.85	4.20
75^{th} Perc.	7.32	4.11	5.18	3.81	5.38
Skewness	-0.21	-0.14	-0.34	-0.05	-0.42
Kurtosis	-0.53	-1.06	-0.58	-0.65	0.08

Table 2. Zonal statistics of vegetation MSPA in 2021 and the SUHI intensity in K (1)

Statistics	Loop	Bridge	Branch	Bo.-O	C-O
Mean	2.54	3.52	4.77	2.15	3.15
Std	2.87	2.43	2.37	2.25	2.36
Variance	8.26	5.91	5.60	5.07	5.57
Area (km²)	0.008	0.01	0.14	1.87	0.41
25^{th} Perc.	0.21	1.85	3.37	0.27	1.39
50^{th} Perc.	2.65	3.74	4.97	2.08	2.96
75^{th} Perc.	3.73	5.05	6.17	3.66	4.85
Skewness	-0.18	-0.42	-0.34	0.30	0.25
Kurtosis	-1.10	-0.35	0.19	-0.47	-0.41

Table 3. Zonal statistics of vegetation MSPA in 2021 and the SUHI intensity in K (2)

3.3 Generation of new green areas

The generation of different NbS set ups was carried out in the city of Milan, considering the most susceptible locations based on the SUHI intensity and susceptibility maps, and the current vegetated locations. Two set ups were created to test the methodology.

- The first set up was the simulation of green roofs. The generated green roofs cover an area of 0.7 km^2 within a bounding box of 5.6 km^2, see figure 11. The new areas were sampled from the land cover residential class and refined with the building height dataset to consider only the roofs, removing non urban areas, e.g., streets and inner yards. The selection of a continuous set up is based on the cooling capacity of core patterns.

Figure 11. Locations of simulated green roofs.

- The second set up was the simulation of green corridors (see figure 12), i.e., creating buffers surrounding all the MSPA vegetation cores and creating bridges connecting the nearby vegetation areas, including urban vegetation, agricultural and forest areas. The bridges were created only if the distance between the vegetation cores is less or equal than the buffer size. The buffers and bridges were refined with the land cover dataset to exclude water pixels. The selected buffer size was 5 meters covering an area of 4.6 km^2.

Figure 12. Locations of simulated 5-meter green corridor.

3.4 Measuring the impact of the new vegetation

The SUHI intensity ANN regression model was used to evaluate the behaviour of the phenomenon after introducing land cover changes in the AOI.

The simulated green roofs adopted the average NDVI, NDBI, and albedo values of the urban vegetation land cover class. These were 0,57, -0.17, and 0.15, respectively. The simulation of the green roof set up suggests that the mean SUHI intensity decreased more than 5K with a less variable distribution, see table 4 for further information.

Prediction (K)	Mean	Median	Std	Min	Max
Original	8.4	8.7	1.8	0.11	13.4
Green roofs	3.3	3.3	0.6	-0.06	5.3

Table 4. Original SUHI intensity vs. green roofs SUHI intensity in a sample area.

In a similar fashion, the green corridor's impact on the SUHI intensity was measured and the results reported in table 5. Highlighting that the new vegetation areas are connected with core vegetation areas, the SUHI intensity decrease was around 1K.

Prediction (K)	Mean	Median	Std	Min	Max
Original	2.7	2.7	2.5	-3.6	15.2
Green corridor	1.4	1.1	1.33	-0.5	7.7

Table 5. Original SUHI intensity vs. green corridors SUHI intensity in a sample area.

4. Discussion

The produced SUHI susceptibility and intensity maps showcase the behaviour of this phenomenon in summer, with respect to the average spectral conditions of 2020-2022. The SUHI susceptibility map illustrates the overall behaviour throughout the years. The SUHI concentrates in the city center and in the northern parts of the metropolitan area, where the population density is higher. Moreover, the SUHI intensity map explains the spatial distribution of the temperature difference across the susceptible areas, with an overall range from -5K to 10K.

The zonal statistics of the SUHI intensity, based on the MSPA vegetation classes, demonstrate how the core vegetation areas have the highest cooling capacity. Based on the previous fact, two NbS set ups were proposed: core green roofs, and the extension of the current vegetation cores with green corridors.

The green roofs simulation provided a mean and maximum SUHI intensity mitigation of 5K and 8K, respectively, with a 3.3K mean SUHI intensity; which is consistent with the results of similar studies (Asadi et al., 2020).

The green corridors simulation, consisting of 5-meter buffered vegetation cores and connecting bridges, slightly mitigated the phenomenon in areas where the SUHI intensity was already low due to their adjacency with cores of vegetation. It is relevant to mention that the bridges follow an Eucledian path rather than a natural path. However, this fact can be neglected considering the maximum length of the bridges.

5. Conclusion

A machine learning-based methodology for modelling Surface Urban Heat Island (SUHI) phenomenon was proposed. The methodology is bi-folded. The first part regarded the modelling of the SUHI susceptibility to provide a general overview of

the SUHI behaviour throughout the years, and the SUHI intensity to to provide a spatial overview of the LST dynamics. The second part focused on the simulation of Nature based Solutions (NbS) to assess their impact with respect to SUHI intensity, by re-evaluating the previously produced model.

The case study of Milan (Italy) was presented with an initial assessment of the Land Surface Temperature (LST) and Land Cover (LC) dynamics to enhance the understanding on the SUHI phenomenon during summer. In the same context, the Morphological Spatial Pattern Analysis (MSPA) of vegetation was derived from the LC dataset to characterise the geometry and connectivity of the vegetation landscape. The main vegetation MSPA classes were cores and edges.

The SUHI susceptibility and intensity were modelled based, among other data, on Landsat-8 imagery. The selected machine learning method was the Artificial Neural Network (ANN) for both classification and regression tasks, resulting in an accuracy of 87% and mean absolute error of 2.65K. The models were used to produce the SUHI susceptibility and intensity maps in the metropolitan area of Milan to showcase the spatial behaviour of the phenomenon in a larger area of interest.

The produced SUHI intensity model served as a basis for evaluating the effect of land cover changes to mitigate the SUHI. In fact, the spatial set up of two NbS were provided based on their possible potential mitigation effects. The first was the simulation of green roofs covering a 0.7 km^2 area, and the second, the simulation of green corridors covering a 4.6 km^2 area. Their impact on mitigating SUHI intensity were around 5k and 1k, respectively. Other set-ups can be tested based on specific scenarios.

The proposed methodology can be easily implemented in other places by relying on global data sources such as Urban Atlas for Land Use/Land Cover. Although, local and frequently updated datasets are recommended for more precise results.

5.1 Limitations and future work

-The study is limited to the modelling of the SUHI in the summer season. Other seasons may be analysed to understand the SUHI dynamics thoughout the year.

- The study is limited to the modelling of the SUHI since 2015. A deeper analysis could be carried out considering more years into the past based on the data availability.

- The current model, ANN, can be replaced by more advanced models such as Convolutional Neural Networks or Transformers for capturing better the spatial behaviour of the SUHI.

References

Asadi, A., Arefi, H., Fathipoor, H., 2020. Simulation of green roofs and their potential mitigating effects on the urban heat island using an artificial neural network: A case study in Austin, Texas. *Advances in Space Research*, 66(8), 1846-1862.

Bentivoglio, R., Isufi, E., Jonkman, S. N., Taormina, R., 2022. Deep learning methods for flood mapping: a review of existing applications and future research directions. *Hydrology and Earth System Sciences*, 26(16), 4345–4378.

Calhoun, Z. D., Willard, F., Ge, C., Rodriguez, C., Bergin, M., Carlson, D., 2024. Estimating the effects of vegetation and increased albedo on the urban heat island effect with spatial causal inference. *Scientific Reports*, 14.

He, Y., Lin, E. S., Yu, Z., Tan, C. L., Tan, P. Y., Wong, N. H., 2021. The effect of dynamic albedos of plant canopy on thermal performance of rooftop greenery: A case study in Singapore. *Building and Environment*, 205.

Lu, H., Gaur, A., Lacasse, M., 2024. Climate data for building simulations with urban heat island effects and nature-based solutions. *Scientific Data*, 11(1), 731.

Pugliese Viloria, A. d. J., Folini, A., Carrion, D., Brovelli, M. A., 2024. Hazard Susceptibility Mapping with Machine and Deep Learning: A Literature Review. *Remote Sensing*, 16(18). https://www.mdpi.com/2072-4292/16/18/3374.

Soille, P., Vogt, P., 2009. Morphological segmentation of binary patterns. *Pattern Recognition Letters*, 30(4), 456-459.

Soille, P., Vogt, P., 2022. MORPHOLOGICAL SPATIAL PATTERN ANALYSIS: OPEN SOURCE RELEASE. *The International Archives of the Photogrammetry, Remote Sensing and Spatial Information Sciences*, XLVIII-4/W1-2022, 427–433.

Vogt, P., Riitters, K., 2017. GuidosToolbox: universal digital image object analysis. *European Journal of Remote Sensing*, 50(1), 352–361.

6. Appendix

The Landsat-8 L2C2 scenes were downloaded from the USGS EarthExplorer through the Landsatxplore Python package. The specific scenes dates are listed per year in the following in MM/DD format.

- 2015 (3): 07/06,07/22,08/07.
- 2016 (2): 06/22,08/25.
- 2017 (1): 05/24.
- 2018 (2): 07/30,08/15.
- 2019 (1): 07/17,08/18.
- 2020 (2): 07/19,08/20.
- 2021 (2): 07/06,07/15.
- 2022 (3): 07/21,08/02,08/18.